Oct 18th, 12:00 AM

Behaviour of Cold-formed SHS Beam-columns

Raef M. Sully

Gregory J. Hancock

Twelfth International Specialty Conference on Cold-Formed Steel Structures
St. Louis, Missouri, U.S.A., October 18-19, 1994

BEHAVIOUR OF COLD-FORMED SHS BEAM-COLUMNS

Raef M. Sully[1] Gregory J. Hancock[2]

SUMMARY

This paper describes a test programme conducted into the behaviour of cold-formed, compact square hollow section beam columns. The tests were conducted in a purpose built test rig capable of applying load and moment in a constant ratio. The test specimens were pin-ended specimens loaded, with varying load/moment ratios, at two different ratios of end moment. The results of the tests were simulated using a finite element programme. This finite element programme was used to find maximum second order elastic moments, for the section tested, at varying ratios of end moment. The results of this numerical investigation are compared with the relevent interaction design rules from AS4100 (Standards Australia (1990)) and the AISC-LRFD specification (1986).

[1]PhD research student at the School of Civil & Mining Engineering, The University of Sydney
[2]BHP Steel Professor of Steel Structures, School of Civil & Mining Engineering, The University of Sydney

1 INTRODUCTION

At present in Australia, the design rules applicable to cold-formed tubular beam-columns are simple linear interaction curves (Chapter 8 of AS4100 (Standards Australia(1990)). However within the same standard, advanced interaction rules are available for doubly symmetric, compact I-sections. In the U.S.A., in the AISC Specification (1986), there is a more advanced rule for interaction which applies to all sections whether I or tubular. This curve is lower than the Australian in some cases and higher in others. It was believed that cold-formed tubes would have at least the same capacity as doubly symmetric I-sections, to reach full moment capacity with small axial forces acting in the section. A test programme was therefore conducted to assess; (i) the behaviour of cold-formed, compact square hollow sections, under varying load/moment ratios, for two end moment conditions, and (ii) the applicability of the current advanced interaction rules, in both AS4100 and the AISC Specification, for cold-formed, compact square hollow sections. The test results are compared with an advanced finite element nonlinear analysis developed at the University of Sydney (Clarke et al, (1991,1992,1993)). The advanced analysis is then used to generate design curves for a range of end moment ratios greater than could be performed in the tests.

2 TEST RIG LAYOUT AND OPERATION

A test rig was purpose built for this test programme. It consists of a 2000kN (450 kips) hydraulic actuator used to apply compressive axial force and a 200kN (45 kips) hydraulic actuator used to apply bending moment to the specimen . The moment was applied to the specimens by the bending actuator via lever arms attached to each end of the specimen.

The general layout of the test rig is shown in Figure 1. The layout of the rig allowed for a range of end moment ratios (β) from around β = -1/4 to β = -1 (ie specimens bent in single curvature. The rig does not allow for positive values of β (ie specimens bent in double curvature).

The two actuators could be operated independently or coupled depending on the loading type being investigated. For this test programme, the actuators were linked together so that by controlling one, in either load or displacement, loads would be applied in a constant ratio.

For high compressive load tests, the compression actuator was initially controlled by displacement of a built-on transducer and then towards ultimate by means of an extensometer. While the compressive actuator was being controlled directly, the bending actuator was in load control being controlled from the load signal from the compression actuator. For the high moment cases, the control was reversed. Here the bending actuator was in direct displacement control and the compression actuator was in load control from the bending actuator load signal.

The compression actuator was fitted with both a load cell and a displacement transducer as was the bending actuator. In addition, an extensometer was placed on the test rig to measure actual specimen extension. The southern end frame of the test rig was held in place by four high tensile steel bars as shown in Figure 1, forming a very flexible system. Hence there was a considerable difference between the compression actuator displacement and actual specimen compression. With the compression actuator in extensometer control the effect of the flexible test rig could be compensated for.

Seven transducers were mounted along the length of the specimen to measure lateral displacement, in the plane of bending. They were located at the ends, centre, and at other points along the specimen. For some of the earlier tests, a transducer was also mounted vertically to measure out of plane deflections at mid span. This was found to be virtually zero and was not measured on later tests. Output from the hydraulic

actuator controllers, and the transducers were collected through a data acquisition system.

3 MATERIAL PROPERTIES

3.1 Tensile Coupon Tests

Tensile coupons were cut from both the flats and corners of the section to determine the proof stress ($\sigma_{0.002}$) and the ultimate tensile strength (σ_{ut}). The coupons were prepared and then tested according to Australian Standard AS1391 (Standards Australia (1991)), in a 250 kN (56.2 kips) capacity testing machine. Each tensile coupon was instrumented with two linear strain gauges. During the test, a constant cross head speed of 0.01 cm/min ($2.22 \times 10^{-5} s^{-1}$ category L2, Standards Australia(1991)) was used.

The strain was calculated from the mean of the two strain gauge readings for strains up to 25000 micro strain. The strain gauges failed above strains of this size. Consequently, strains after this point were calculated by first finding the elongation from the cross head speed and time measurements and then dividing by the initial gauge length.

To calculate the stress for the corner coupons, the cross sectional area was calculated by weighing, after testing, a known length of each specimen. Each length was of a constant cross section prior to testing so by knowing the weight and density the cross sectional area was able to be calculated.

Results of the tensile coupon tests are shown in Table 1 where the 0.2% proof stress ($\sigma_{0.002}$) and ultimate stress (σ_{ut}) are shown. The proof stress is calculated by first finding the initial modulus of the the tensile coupons. This was calculated to be approximately 208000 (30168 ksi) MPa for the flat material and 195000 MPa (28282 ksi) for the corner material. The 0.2% proof stress is the then defined as the point where a straight line of slope equal to the initial modulus, and x-intercept of 0.002, intersects with the plotted values of stress versus strain.

3.2 Membrane and Bending Residual Stress Tests

To gain additional information on the material properties of the test sections, tests were conducted to ascertain the level of membrane and bending residual stress within the sections. This was done by attaching linear strain gauges to the inside and outside of a short length of the section used. The section was cut to a length of 300 mm (11.8 in.); short enough to allow fixing of the internal strain gauges, and long enough (>2b) to allow measurement of the full membrane residual stresses, given that they are equal to zero at the free ends of the section.

Eight strain gauges were used in the test (two on each face) as shown in Figure 2. The results of the test are shown in Table 2. The odd numbered gauges were on the outside of the specimen, the even numbered gauges on the inside. The numbers in columns four to seven, of Table 2, are for the face to which the corresponding gauges were attached. For example, the weld face (gauges 1 and 2) had a residual membrane strain of 181 micro strain and a residual bending strain of 1816 micro strain. The residual stresses were calculated from the strains assuming a modulus of 208000 MPa. As can be seen from the figures, the residual membrane stresses were virtually zero. The weld face gauges were close to the weld and so it is assumed that the levels here were a local result of the weld. The bending residual stresses were also consistent. They show substantial tension on the outside and matching compression on the inside. The levels of released bending stress measured were close to yield.

4 TEST RESULTS

4.1 Stub Column Tests

In order to determine the section capacity of the specimens, two stub column tests were carried out in a 2000 kN hydraulic actuator. The top platten was a spherical seat while the bottom platten was fixed. They were controlled using an extensometer mounted externally, measuring longitudinal displacement. The stub column test specimens were cut to a length of 500 mm (19.685 in.) with machined ends. This is within the guidelines set out by Galambos (1988) where the length (l) was within the bounds $3d < l < 20r$ given that d is the largest outer dimension of the cross section and r is the radius of gyration.

A plot of axial displacement against axial load for both tests is shown in Figure 3. As can be seen, both specimens reached similar ultimate loads (1173 kN (263.7 kips)) and 1196 kN (268.9 kips)). However the mode of failure evident in both cases was different. The first (1173 kN) formed a symmetric collapse mechanism with outward facing buckles appearing mid-height on opposite faces. Comparable inward facing buckles formed on the other set of opposite faces, again at mid-height. The second specimen (1196 kN) failed via an assymetric buckling configuration; buckles of different sizes appeared at different heights on each of the faces. The asymmetric mode of failure occurred at a larger axial deformation than the symmetric mode (7.87 mm (0.310 in.) as opposed to 6.75 mm (0.266 in.) for the symmetric case) and was probably due to the machined ends being slightly non-flat.

4.2 Geometric Properties

Overall geometric imperfections were measured for the test specimen used in the column test described in Section 4.4. This was performed using a Wild NA2 level with a GPM3 Parallel Plate Micrometer giving direct readings to 0.1mm (0.0039 in.) and estimations easily to 0.02mm (0.00079in). The test specimen was supported at both ends. Measurements were then taken along the specimen on all four sides. The results were adjusted for the effects of self weight and are plotted in Figure 4. As shown the largest imperfection was around 0.5 mm (0.020 in.). This corresponds to an imperfection of 1 in 6900. The results for opposites sides were averaged to give the plot in Figure 5. Here the maximum imperfection is around 0.4 mm (0.016 in.) or 1 in 8625. These values are comparable with those reported earlier by Key, Hasan and Hancock (1988).

In addition to measuring the overall imperfection, the cross sectional dimensions were measured using a micrometer and a digital vernier. The comparison of nominal versus actual dimensions is set out in Table 3.

4.3 Plastic Bending Test

In order to correctly non-dimensionalise the interaction tests, it was necessary to obtain a reference plastic bending capacity and column strength. The plastic bending test was conducted using another 2000 kN hydraulic actuator in a four point bending test configuration as shown in Figure 6. Vertical plates were welded to the web at the ends and at points 1000 mm (39.37 in.) in from both ends. Horizontal plates were then welded to these to form the loading surfaces. The ends sat on half rounds while a large transfer beam was used to load the two internal loading surfaces.

A plot of curvature versus moment is shown in Figure 7. As shown in Figure 6, three transducers were used to measure vertical deflection in the region of constant moment. The middle transducer was located at mid-span, the other two equidistant from the middle one, allowing a relationship between curvature and

vertical displacement to be calculated as described in Hasan and Hancock (AISC(1989)).

The plastic bending test reached 53 kNm (39.1 Kip ft) at ultimate and, after substantial deformation, was concluded when a local buckle had formed in the specimen. It formed near one of the points of application of load in the constant moment region as expected. Given the compact nature of this section, it was not surprising to see the very large deformations that occurred in the plastic region of the test. At the completion of testing, the specimen had a mid-span deflection of around 230 mm (9.06 in.) (equivalent to a deflection to span ratio of 1/12).

4.4 Column Test

A column test was conducted in the test rig by application of the compression actuator only. The column specimen was 3000 mm (118.1 in.) long giving it an effective length of 3450 mm (135.8 in.). An eccentricity of 3 mm (0.12 in.) was added at each end in the plane of bending. This was considerably greater than the measured geometric imperfection of 0.4 mm (0.016 in.).

A graph showing load versus central moment is shown in Figure 9. The specimen exhibited stable unloading characteristics, after reaching an ultimate axial load, P_{uc}, of 632 kN (142.1 kips). At this load, there was significant moment induced in the specimen from the P-Δ effect, as shown in Figure 9.

4.5 Interaction Tests

All of the specimens tested were 3000 mm (118.1 in.) long. Adding this to the 225 mm (8.86 in.) at each end of the test rig, from the centre of the pins to the ends of the test specimen, gave the columns an effective length of 3450 mm (135.8 in.) between the pinned bearings. This length was chosen because it gave a non-dimensionalised slenderness (λ) of approximately 1 when the nominal yield stress (σ_y = 350 MPa (50.763 ksi)), and nominal dimensions were used.

$$\lambda = \left(\frac{L_e}{r}\right).\sqrt{\frac{\sigma_y}{\pi^2 E}} \tag{1}$$

Two series of interaction beam-column tests were conducted. For the first series with β=-1 (referred to as B1 series), four tests were conducted with varying ratios of applied load and moment. In order of descending applied load/moment ratio they are B1R1 to B1R4. For the second series with β=-0.5 (referred to as B2 series), three test were conducted, known as B2R1 to B2R3, again in descending order of applied load/moment ratio.

Plots of load versus central moment for the four B1 series of tests are shown in Figure 8. This central moment is the sum of the moment applied directly from the bending actuator and the moment indirectly applied via the P-Δ effect from both the compression and bending actuators.

All of the tests exhibited substantial ductility. The high load/moment ratio tests showed a significant increase in bending moment after the maximum load was reached. All of the tests were concluded when the bending actuator ran out of travel. No local buckling was observed despite the large lateral deflections experienced; (for B1R1-73mm (2.87 in.), B1R2-165mm (6.50 in.), B1R3-135mm (5.31 in.), B1R4-71mm (2.80 in.)). It is interesting to note that tests B1R2 to B1R4 all reached the plastic bending capacity. In the case of B1R2, this was with an axial load of approximately 250 kN (56.2 kips) or 40% of it's column capacity.

The curves for all four B1 series tests are linear to begin with as would be expected. The curves then flatten out due to the P-Δ effect at mid-span. The effect is more significant for the high load/moment ratio tests (B1R1 and B1R2) and almost non-existent for B1R4. In the case of B1R4, the only axial load contributing to the P-Δ effect is that load coming directly from the bending actuator (this test was conducted with zero load on the compression actuator).

Plots of load versus maximum moment for the B2 series are shown in Figure 9. These tests similarly showed that the section plastic moment capacity could be reached for loads below approximately 25% of the column capacity. However for higher load/moment ratios (over about 50% of column capacity) the failure envelope for the B2 series of tests is up to 20% greater in load capacity than for the B1 tests. This is most probably due to the different moment gradients in the specimens in the B2 series, and the subsequent lessening of the P-Δ effect.

Unlike the B1 series, the region of maximum moment for the B2 series shifted during the tests . At low loads, the peak moment was at the point of application of greatest applied moment, ie at the southern end. As the deflections increased, the P-Δ effect increased and the peak moment shifted northward towards the centre of the specimen. The extent to which the shift occurred was dependent on the applied load/moment ratio. Test B2R1 buckled locally just south of midspan. By comparison, test B2R3 buckled locally approximately 100 mm (4 in.) north of the point of application of maximum moment. Test B2R2 showed no local buckle at the time the moment actuator ran out of travel, causing the termination of the test.

The plot of load versus moment for the column test is included in the plot of load versus moment for the B2 series of tests (Figure 9).

5 ANALYSIS

An advanced finite element non-linear analysis, developed at the University of Sydney by M. Clarke (Clarke et al, (1991,1992,1993)) was used to simulate each of the tests. The advanced analysis can include the effects of large deflections, residual stresses, material non-linearity, gradual yielding, elastic unloading, and geometric imperfections.

The finite element analysis uses an isoparametric curved beam element. It includes total Lagrangian, updated Lagrangian and co-rotational formulations for the geometric non-linearity. To incorporate inelastic material behaviour, a distributed plasticity approach is used. This involves the cross-section being discretised into a fine grid of monitoring points, also facilitating the inclusion of residual stresses.

Material properties for the finite element analysis were taken from the results of the tensile coupon tests and residual stress tests. Material curves were multi-linear functions derived directly from the stress strain curves. Membrane residual stresses were taken as zero. The end plattens were included as a third material type to account for their increased stiffness. Measured eccentricities between the specimens and the end plattens were included. Geometric imperfections were taken as sinusoidal over the length of the specimen with a mid span deflection of 0.4mm. This is similar to that shown in Figure 5.

Good agreement is shown between the analysis and tests results for stub column (Figure 3), beam (Figure 7), and column tests (Figs. 9). The finite element program cannot model local buckling of the specimens. For this reason, the analysis does not follow the unloading behaviour of the stub column and beam tests. In both of these tests, local buckling precipitated the falling behaviour. In the column test, however, overall buckling is responsible for the unloading behaviour shown.

Comparison of analysis and tests results for the B1 series of interaction tests is shown in Figure 8. Again

there is good agreement especially for tests B1R3 and B1R4. The specimen used for B1R2 had been previously loaded very close to ultimate in another test (at the same load moment ratio).The test had then been abandoned due to technical problems. The analysis shown included material curves allowing for the strain hardening that occurred in the first test, and geometric imperfections commensurate with the plastic deformation the specimen underwent. For test B1R1, it should be noted that one of the small manual hydraulic jacks used to position the specimens vertically was not released at a small axial load as was normally done. At maximum load it was noted to be applying some longitudinal force into the specimen. It was then released. This is possibly the reason the difference between test and analysis is greater here than for other tests.

Figure 9 shows the comparison between test results and analysis for the B2 series of interaction tests. There is good agreement here for all three tests. The only problem again being that the finite element program used does not have the capability to allow for local buckling, as occurred at the end of tests B2R1 and B2R3. Processing the analysis results allowed the maximum moment and its position to be calculated. The location of the maximum moment, as well as its magnitude, obtained from the analysis agreed well with test results.

6 DESIGN

To compare the test results with current design rules, further finite element analyses were undertaken, for β=-1, β=-1/2, β=0, β= 1/2, and β=1. From each of these analyses, the maximum applied load was found with the corresponding maximum applied end moment. Using equations 7.3 and 7.4 from page 260 of Trahair and Bradford (1977) the equivalent maximum second order elastic moment within the section was calculated. This is of course very different from the actual maximum moment within the section, which is the sum of the applied maximum end moment and moment due to the mid span deflection and load. These maximum second order elastic moments were compared with the current interaction design rules in Clause 8.4.2.2 of AS4100 (Standards Australia (1990)), for doubly symmetric compact I-sections and the interaction rule from the AISC Specification (AISC (1986)). Graphs of these plots for β = -1, β = -1/2, β = 0, β = 1/2, and β = 1 are shown in Figures 10, to 14 respectively.

The graphs have been non-dimensionalised against the short column load P_{sq}, and the plastic moment capacity M_{pt}. P_{sq} is calculated from the measured cross-sectional area and the proof stress of the material from the flats, determined from the tensile coupon tests (Table 1). M_{pt} is calculated using the measured section dimensions to determine the actual plastic section modulus, and the proof stress of the material from the flats, determined from the tensile coupon tests (Table 1). The proof stress was used, in calculating M_{pt} rather than the ultimate tensile stress for two reasons; (i) this method is closer to current design philosophy and, (ii) the curvatures evident in the experimental test at ultimate (0.3 m^{-1} (0.0076 $in.^{-1}$)), while large, are substantially smaller than those corresponding to the ultimate tensile stress (2 m^{-1} (0.050 $in.^{-1}$)). Curvatures this large cannot be attained experimentally before local buckling occurs.

As an alternative, M_{pt} could be calculated using the proof stress from the corners as well as the proof stress from the flats. A comparison, for the β = -1 case only, is included in Figure 10. Calculating M_{pt} using the proof stress from the flats and corners gives a value of M_{pt} closer to that found experimentally. However the derivation is more involved and there do not appear to be any disadvantages in using only the flat material, in design applications. This is also in accord with the material standards for tubes (Standards Australia (1993), and the American Society for Testing Materials (1984)) where the tensile yield stress is based on material from the flats.

7 CONCLUSION

The cold formed, compact square hollow sections tested showed good ductility and good capacity to absorb moment past maximum axial load. Comparing the equivalent second order elastic moments with the design rules, shows that even at β=-1 there is some capacity to absorb small axial forces without reducing the moment capacity. This effect increases with an increase in β. The current interaction design rules in AS4100 (Standards Australia (1990)), for doubly symmetric I-sections are applicable to cold-formed square hollow sections. They are however conservative for larger values of β and there is scope for improved design rules to be developed. The current interaction rules in the AISC specification (AISC(1986)) are more conservative than the theoretical and experimental values except for the β = -1 case.

8 ACKNOWLEDGEMENTS

The authors wish to thank Tubemakers (Aust) Pty Ltd for the tube sections used in this experimental report. The first author also wishes to make known his appreciation for the financial support provided by the J.W. and I.C.M. Roderick Research Bequest and The Centre For Advanced Structural Engineering.

9 APPENDIX REFERENCES

American Institute of Steel Construction (1986), "Manual of Steel Construction, Load & Resistance Factor Design", first edition, 1986.

American Society for Testing Materials (1984), "Cold-formed Welded and Seamless Carbon Steel Structural Tubing in Rounds and Shapes", ASTM-A500.

Clarke, M.J. and Hancock, G.J. (1991), "Finite-Element Nonlinear Analysis of Stressed-Arch Frames", *Journal of Structural Engineering*, American Society of Civil Engineers, Vol. 117, No. 10, 1991, pp.2819-2837

Clarke, M.J., Bridge, R.Q., Hancock, G.J., and Trahair, N.S. (1992), "Advanced Analysis of Steel Building Frames", *Journal of Constructional Steel Research,* Vol. 23, Nos 1-3, 1992, pp. 1-29

Clarke, M.J. (1993), "Plastic-Zone Analysis of Frames", Chapter 6 in *Advanced Analysis of Steel Frames; Theory, Software and Applications,* eds. W.F.Chen and S.Toma, CRC Press, Inc., Boca Raton, Florida, pp. 259-319, 1993.

Galambos, T.V. (1988), *Guide To Stability Design Criteria For Metal Structures*, Wiley Inc, pp 708-710.

Hasan, S.W., and Hancock, G.J. (1989), "Plastic Bending Test of Cold-Formed Rectangular Hollow Sections", *Journal of the Australian Institute of Steel Construction*, Vol. 23, No. 4.

Key, P.V., Hasan, W., and Hancock, G.J. (1991), "Column Behaviour of Cold-Formed Hollow Sections", *Journal of Structural Engineering*, ASCE, Vol 114, No. 2, Feb 1988.

Standards Australia (1990), "Steel Structures", AS4100-1990.

Standards Australia (1991), "Methods For Tensile Testing of Metals", AS 1391-1991.

Trahair, N.S., and Bradford, M.A. (1977), "The Behaviour and Design of Steel Structures", second edition, Chapman Hall,1977.

10 APPENDIX NOTATION

b	External width of section.
E	Modulus of elasticity.
d	External depth of section.
I	Second moment of area.
L_e	Effective length of specimen.
M_{pt}	Full plastic moment capacity.
P	Axial load.
P_{sq}	Short column load.
P_{uc}	Ultimate column capacity.
P-Δ	Moment applification from axial load (P) and deflection of specimen.
r	Radius of gyration.
t_f	Thickness of flange.
t_r	Thickness of corner (or round).
β	Ratio of end moments so that -1 represents single curvature.
λ	Non-dimnesionalised slenderness.
σ	Stress.
σ_y	Nominal yield stress.
$\sigma_{0.002}$	0.2% proof stress.
σ_{ut}	Ultimate tensile stress.
ϵ	Strain.
ϵ_{ut}	Strain at ultimate stress.

Tensile Coupon	$\sigma_{0.002}$ (MPa (ksi))	σ_{ut} (MPa (ksi))	ϵ_{ut} (micro strain)
Flats			
1*	420 (60.92)	453.7 (65.80)	21730
3	379 (54.97)	441.7 (64.06)	N/A
5	393 (56.57)	428.4 (62.13)	N/A
7	376 (54.53)	430.5 (62.44)	N/A
Corners			
2	485 (70.34)	516.4 (74.90)	18440
4	492 (71.36)	519.8 (75.39)	17580
6	496 (71.94)	522.4 (75.77)	17520
8	503 (72.95)	532.1 (77.17)	18690

Table 1: Tensile coupon results.

Strain Gauge	*Reading*		*Residual Membrane*		*Bending*	
	Initial	*Final*	*Strain*	*Stress*	*Strain*	*Stress*
	($\times 10^{-6}$)	($\times 10^{-6}$)	($\times 10^{-6}$)	(MPa (ksi))	($\times 10^{-6}$)	(MPa (ksi))
1	16107	14110				
2	16673	18309	181	38 (5.51)	1816	378 (54.78)
3	16310	14756				
4	15782	17380	-22	-4.6 (-0.67)	1576	328 (47.54)
5	16511	14752				
6	16243	17895	53	11 (1.60)	1706	355 (51.47)
7	15712	14088				
8	16622	18287	-21	-4.4 (-0.64)	1644	342 (49.60)

Table 2: Membrane and bending residual stress.

Dimension	*Nominal* (mm (in))	*Actual* (mm (in))	*Standard Deviation* ± (mm (in))
B,D	125 (4.921)	125.7 (4.949)	0.5 (0.020)
t_f	6.0 (0.236)	5.94 (0.234)	0.08 (0.0032)
t_r	6.0 (0.236)	6.16 (0.243)	0.03 (0.0012)

Table 3: Nominal vs actual cross section dimensions for SHS.

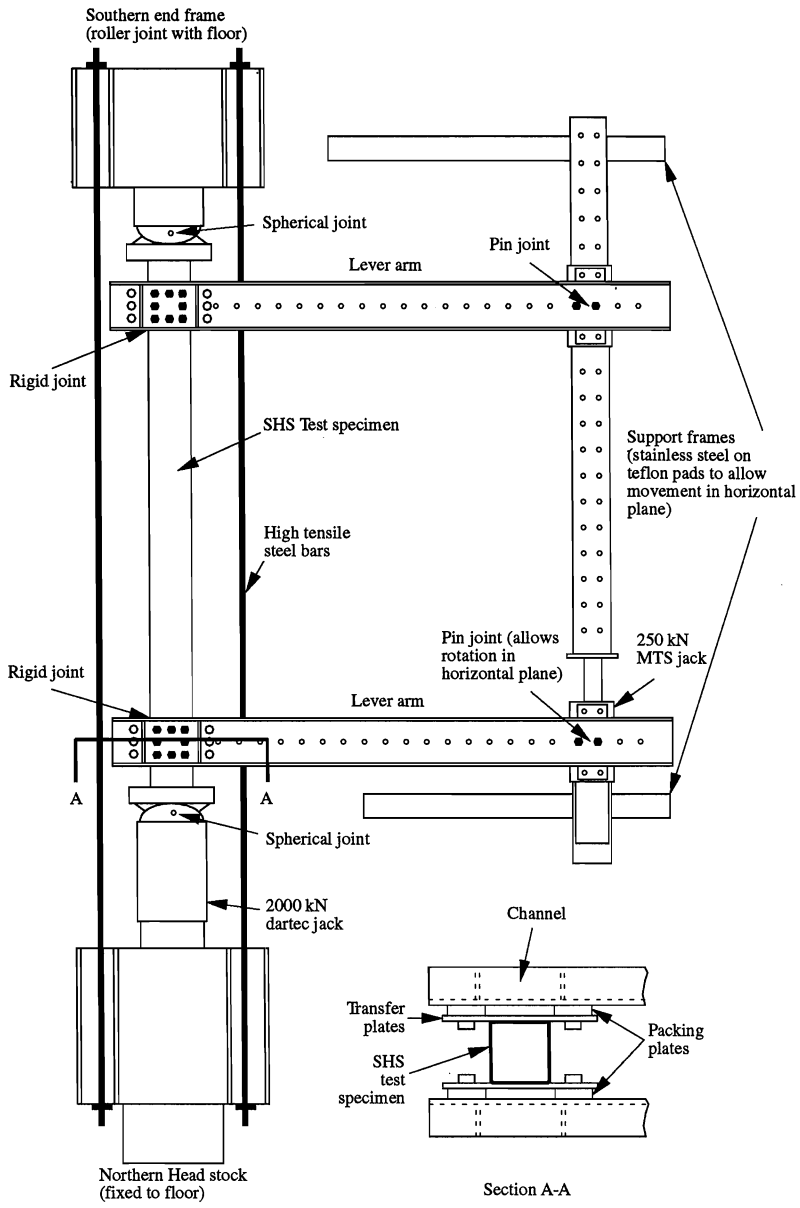

Figure 1: Plan view of test rig layout.

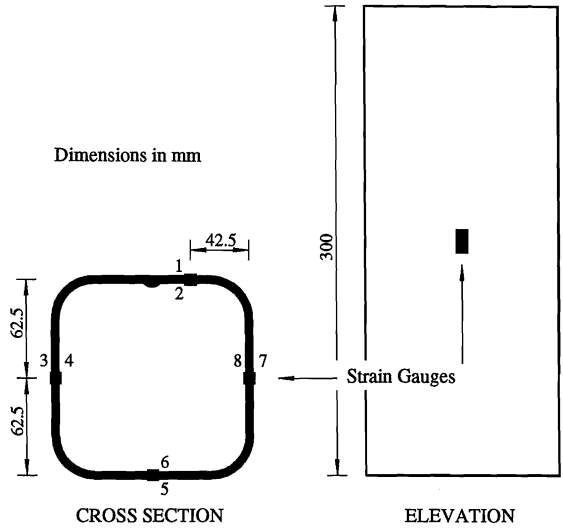

Figure 2: Location of strain gauges for residual stress test.

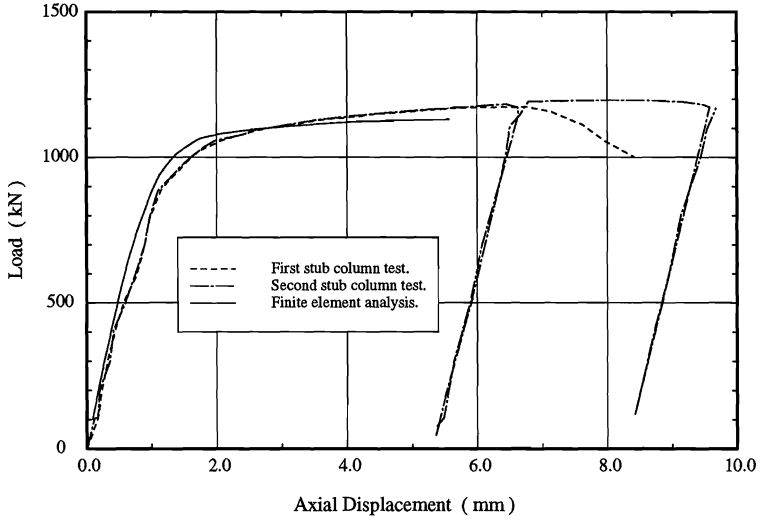

Figure 3: Axial displacement vs load for stub column tests.

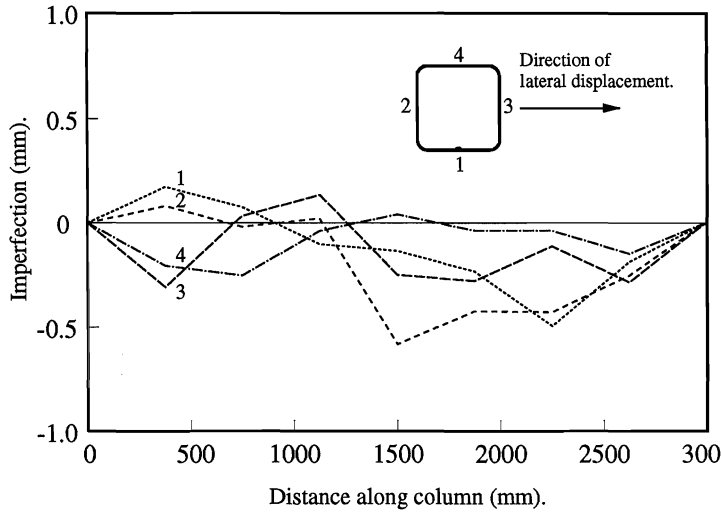

Figure 4: Geometric imperfections for column section on all sides.

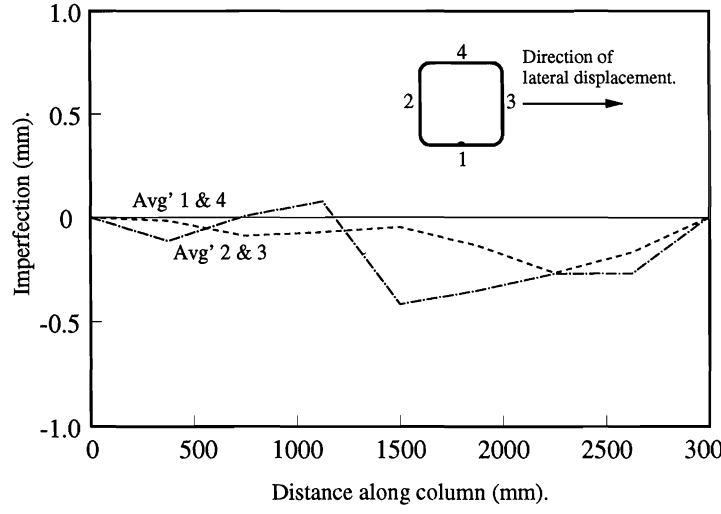

Figure 5: Geometric imperfections for column section averaged for opposing sides.

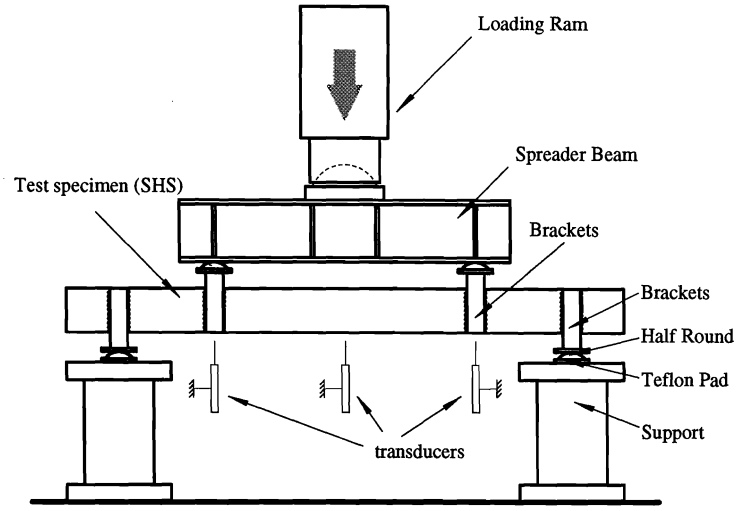

Figure 6: Layout for bending test.

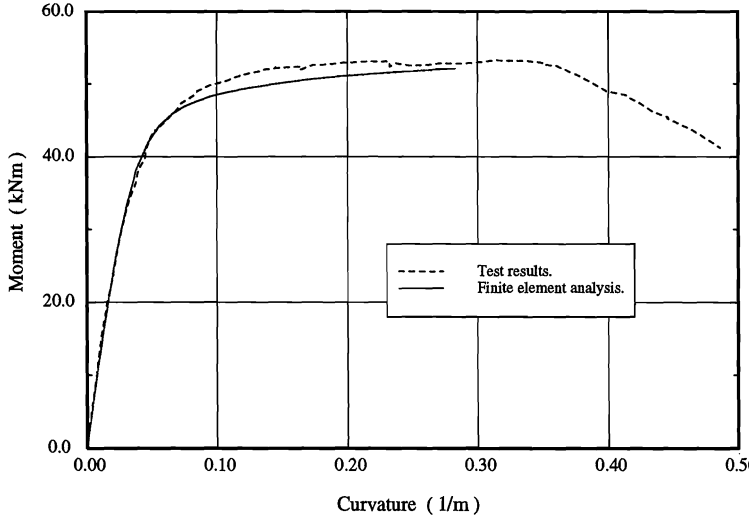

Figure 7: Curvature vs moment for pure bending test.

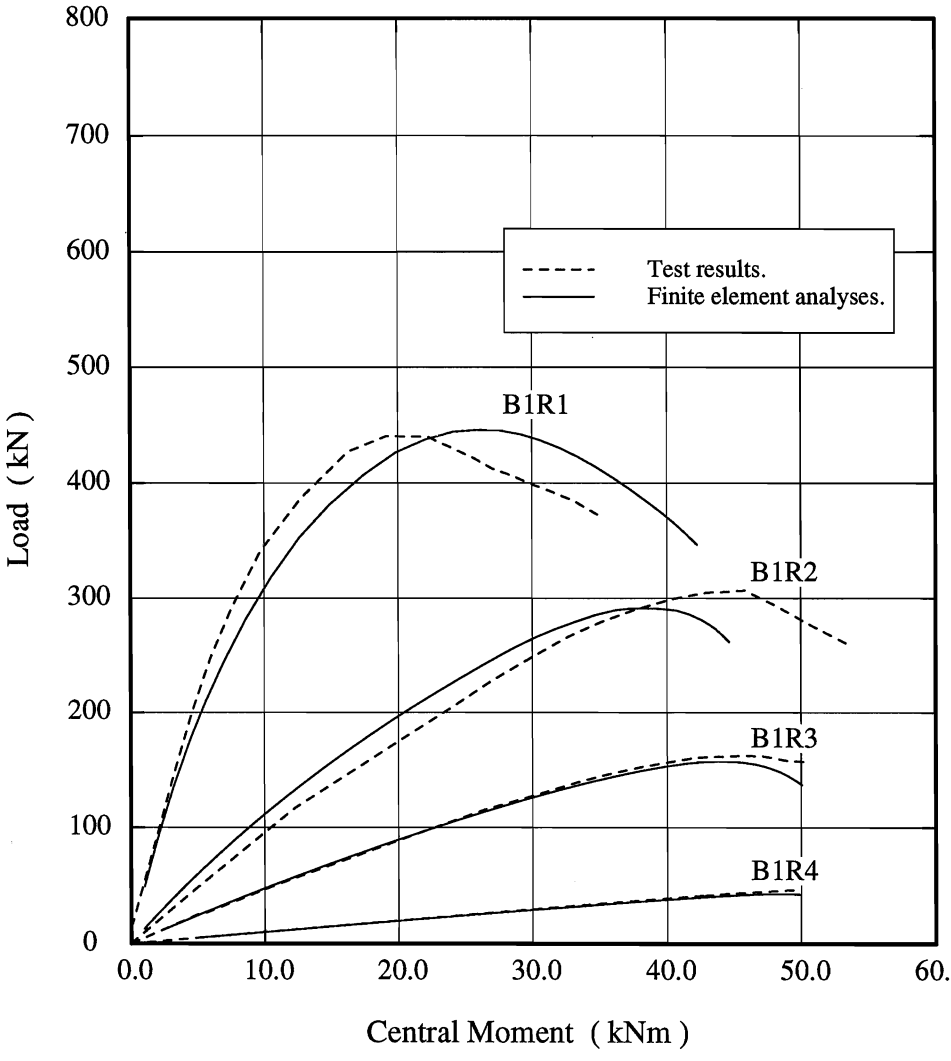

Figure 8: Maximum moment vs load for B1 series of interaction tests.

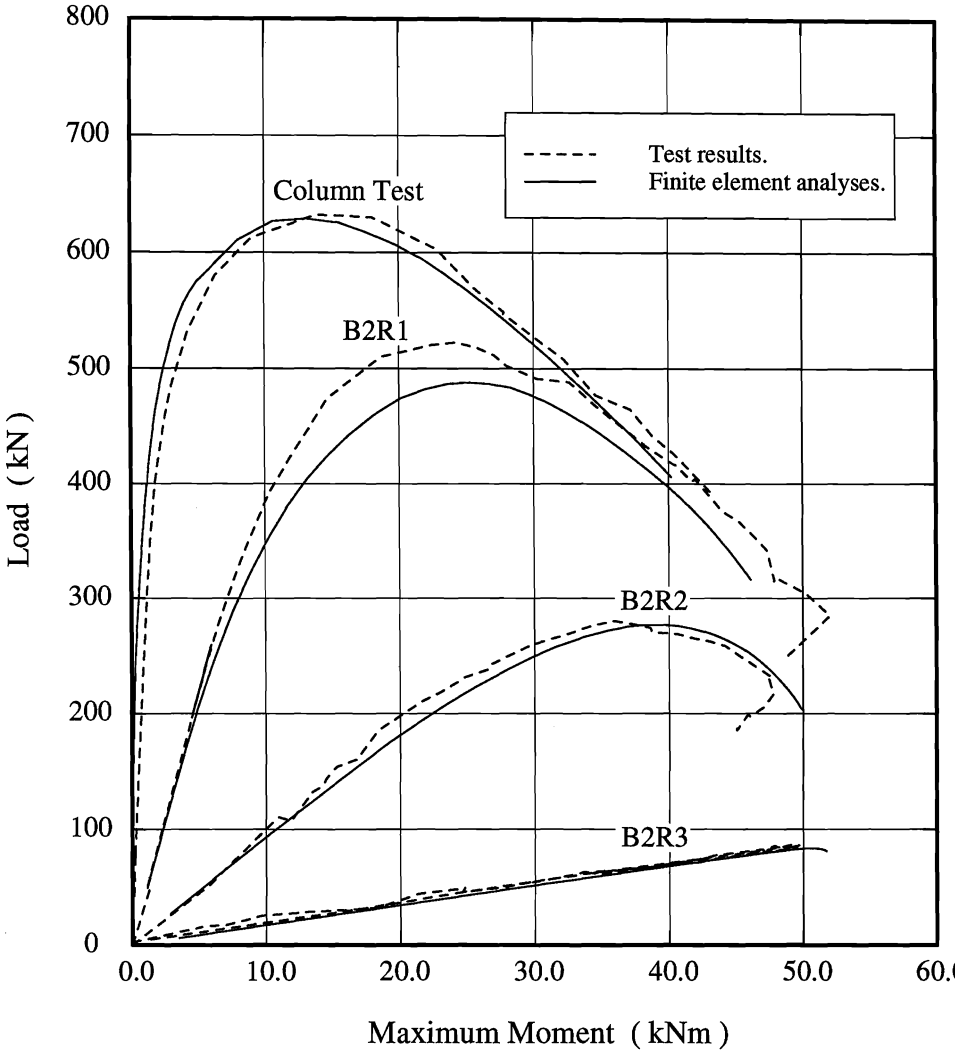

Figure 9: Maximum moment vs load for B2 series of interaction tests.

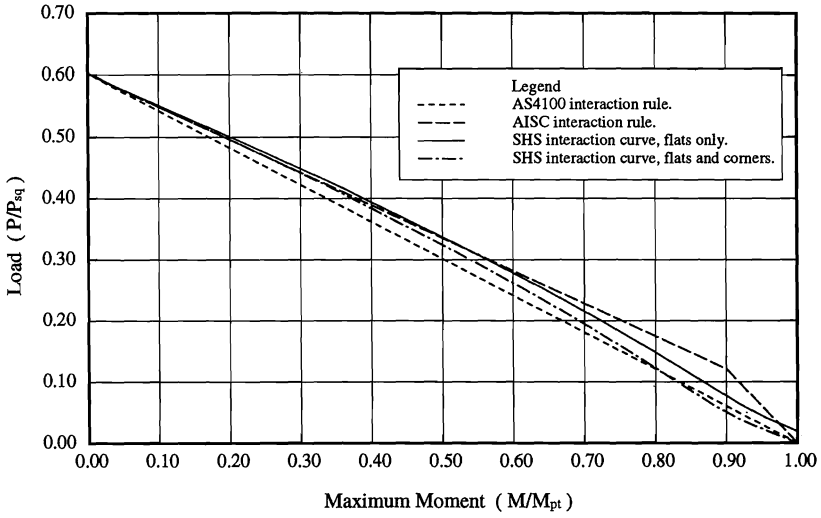

Figure 10: Comparison of design rules with interaction surface for β = -1.

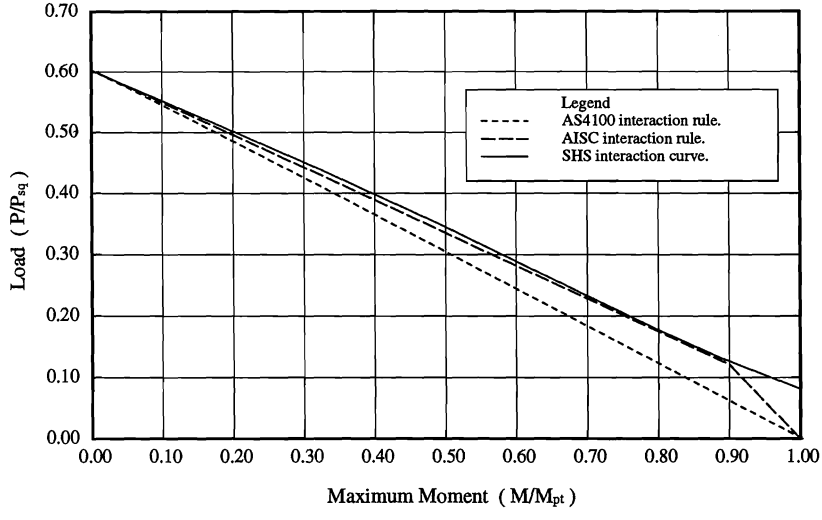

Figure 11: Comparison of design rules with interaction surface for β = -1/2.

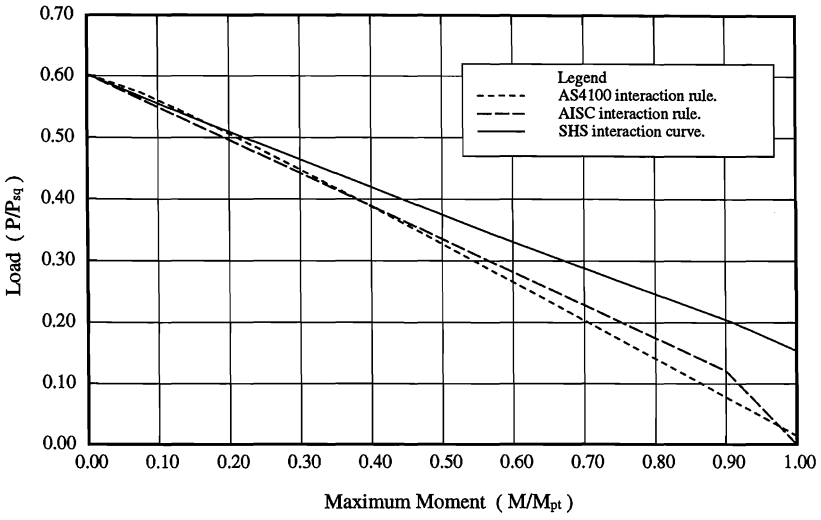

Figure 12: Comparison of design rules with interaction surface for $\beta = 0$.

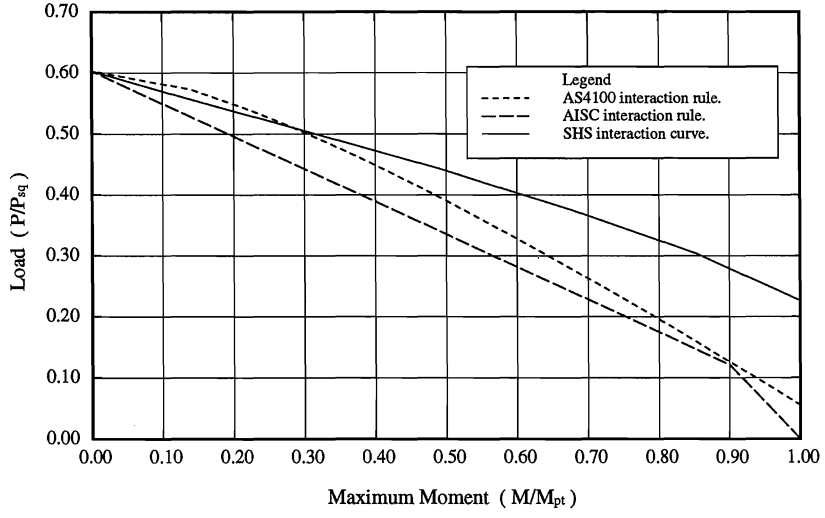

Figure 13: Comparison of design rules with interaction surface for $\beta = 1/2$.

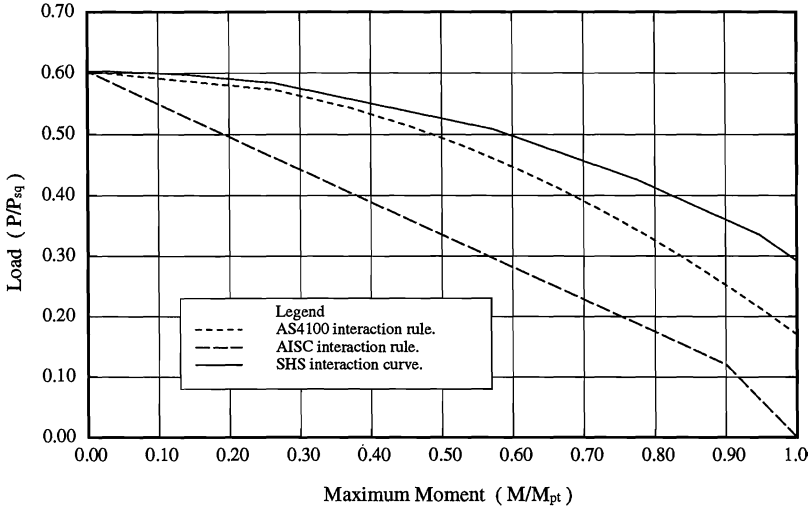

Figure 14: Comparison of design rules with interaction surface for $\beta = 1$.